Arch. Metall. Mater. **69** (2024), 1, 67-72

DOI: https://doi.org/10.24425/amm.2024.147787

HYUN-WOO SHIM[1†], BYOUNGYONG IM[2,3†], SOYEONG JOO[2], DAE-GUEN KIM[2*]

FACILE SYNTHESIS AND Li-ELECTROACTIVITY OF COBALT OXIDE BASED ON RESOURCES RECOVERED FROM WASTE LITHIUM-ION BATTERIES

In this study, cobalt oxide (Co_3O_4) powder was prepared by simple precipitation and heat-treatment process of cobalt sulfate that is recovered from waste lithium-ion batteries (LIBs), and the effect of heat-treatment on surface properties of as-synthesized $Co(OH)_2$ powder was systematically investigated. With different heat-treatment conditions, a phase of $Co(OH)_2$ is transformed into CoOOH and Co_3O_4. The result showed that the porous and large BET surface area (ca. 116 m^2/g) of Co_3O_4 powder was prepared at 200°C for 12 h. In addition, the lithium electroactivity of Co_3O_4 powder was investigated. When evaluated as an anode material for LIB, it exhibited good electrochemical performance with a specific capacity of about 500 mAh g^{-1} at a current density of C/5 after 50 cycles, which indicates better than those of commercial graphite anode material.

Keywords: Waste lithium-ion battery; Recycling; Co_3O_4 powder; Anode material

1. Introduction

Because of remarkable electrochemical characteristics such as high energy density, a low rate of self-discharge, a long-life cycle, and high potential, the demand for lithium-ion batteries (LIBs) is increasing rapidly. This trend can cause instability in the supply and demand of materials for battery manufacturing.

The recycling of waste LIBs is suggested as the most economical method to gain materials for batteries [1-4]. Waste LIBs contain various valuable metallic elements (e.g., Cu, Al, Li, Co, Ni, etc.); cobalt (23.6 wt%), copper (6.2 wt%), lithium (3.7 wt%), aluminum (2.8 wt%), and nickel (2.7 wt%) [4-6]. The recycling of waste LIBs has been conducted using the process of pyrometallurgy and hydrometallurgy. However, most recycling studies are on resource recovery, and research on the application of recycled resources is necessary.

Cobalt, which is recovered as one of the crucial metallic resources in waste LIBs, is of the critical elements for cathode material of LIBs and is used as an important element industrially in both metal and oxide phases. Especially, cobalt oxides are widely applied in fields such as ion-storage, chemical sensors, solar thermal energy collectors, and electrochromic (EC) devices [7-10]. Various studies on the synthesis of cobalt oxide have been conducted to control the phase, shape, and size, and the synthesis methods have been reported, such as hydrothermal synthesis [11-14], calcination [15-17], low-temperature solution process [18].

In this study, cobalt oxide was synthesized by the precipitation method and, subsequently, heat treatment. The starting material is cobalt sulfate solution recovered from waste LIBs. The synthesis behavior was discussed according to the experimental conditions. In addition, the electrochemical evaluation of Co_3O_4 powder, which was synthesized at optimized conditions, was investigated.

2. Experimental

Co_3O_4 powder was obtained through a simple precipitation method and heat treatment. The recycled $CoSO_4$ solution (SungEel HiTech Co., Korea) and NaOH (98-100.5%, Sigma-Aldrich) were used as a starting material and reductant, respectively, without further purification. The schematic diagram of the synthesis of cobalt oxide is shown in Fig. 1. Initially, NaOH

[1] RESOURCES UTILIZATION RESEARCH DIVISION, KOREA INSTITUTE OF GEOSCIENCE & MINERAL RESOURCES (KIGAM)
[2] MATERIALS SCIENCE AND CHEMICAL ENGINEERING CENTER, INSTITUTE FOR ADVANCED ENGINEERING (IAE), 51 GOAN RD., BAEGAM-MYEON, YONGIN-SI, GYEONGGI 17180, YONGIN, REPUBLIC OF KOREA
[3] SEJONG UNIVERSITY, DEPARTMENT OF NANOTECHNOLOGY AND ADVANCED MATERIALS ENGINEERING, SEOUL, REPUBLIC OF KOREA
† These authors contributed equally to this work
* Corresponding author: dgkim@iae.re.kr

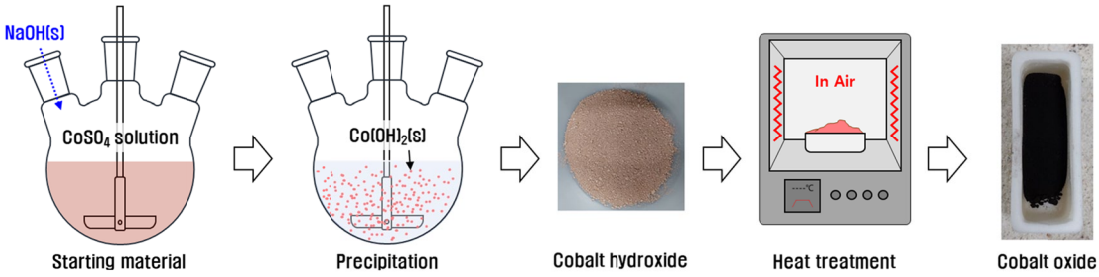

Fig. 1. Schematic diagram for the synthesis of cobalt oxide powder

(80.65 g) was added to the flask containing $CoSO_4$ solution and was thoroughly stirred until the color change of solution to pink. After the reaction, the precipitates were collected and washed with distilled water several times to remove sodium and sulfate ions, and then dried using a freeze dryer for 24 h. Subsequently, the dried powder was calcined at different temperatures (160, 200, and 300°C) and times (1, 3, and 12 h) in the air to study oxidation behavior.

Phase identification and morphology of the samples were characterized by X-ray diffraction (XRD, Shimadzu XRD-6100) and field emission scanning electron microscope (FE-SEM, Tescan-Mira3), respectively. The specific surface area was calculated by the Brunauer-Emmett-Teller (BET, Micromeritics_Trixtar II).

The electrochemical evaluation of Co_3O_4 powder, which was used as the active material of working electrodes versus

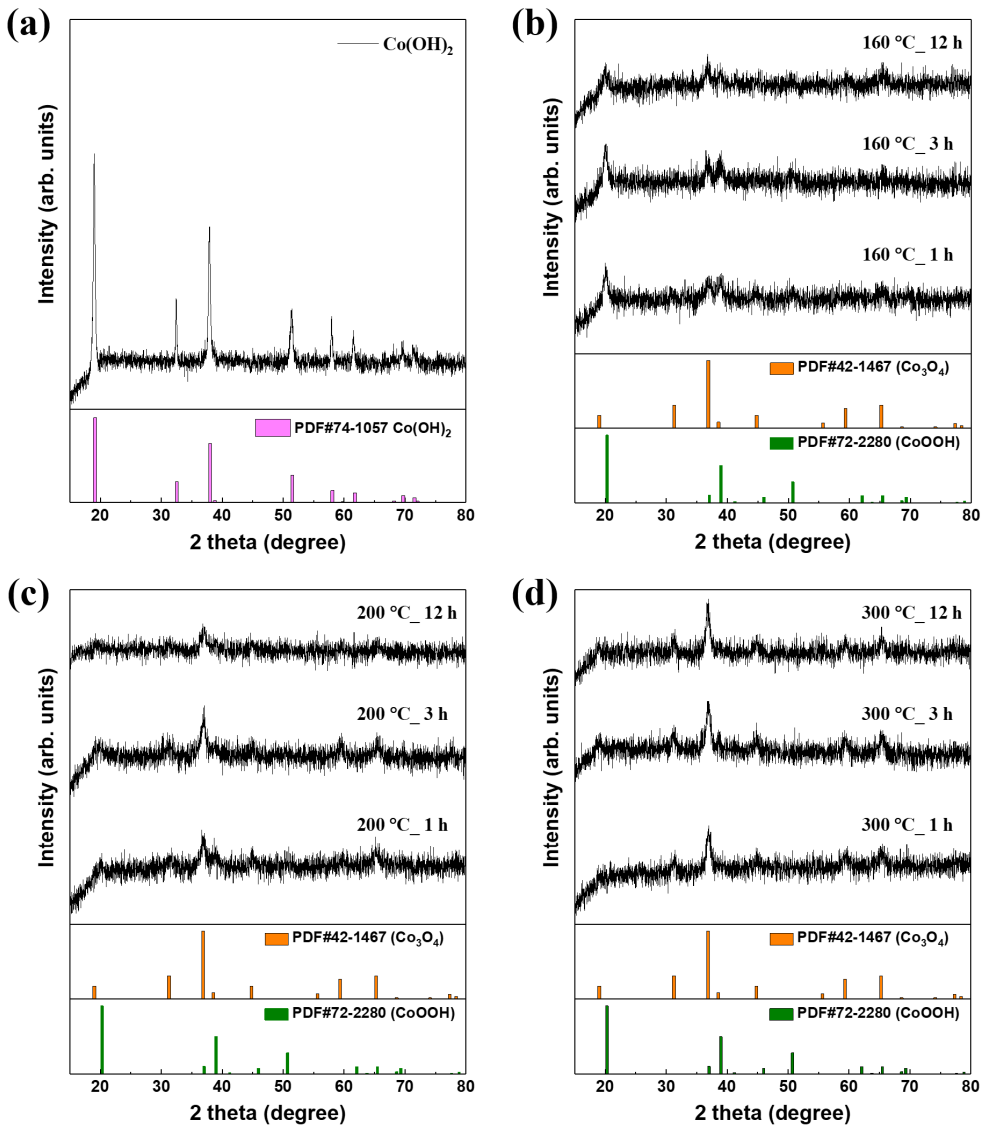

Fig. 2. XRD patterns of the as-synthesized $Co(OH)_2$ powder with different heat-treatment conditions as a function of temperature (heating rate of 10°C/min) and time

lithium metal foil (as a counter electrode), was investigated with cyclic voltammogram (CV) at a scan rate of 0.1 mV s^{-1} and galvanostatic cycling in the potential window of 0.01-3.0 V (*vs.* Li^+/Li). The detailed electrode fabrication and cell assembly procedure have been described elsewhere [19]. All electrochemical measurements were carried out with the assembled half-cells using a battery cycler system (WBCS 3000; WonATech Co., Korea) at room temperature.

3. Results and discussion

XRD patterns were analyzed to determine the crystal structure of all samples. Fig. 2(a) shows the XRD pattern of as-synthesized powder along with the precipitation method. All diffraction peaks were indexed to the hexagonal cell of brucite-like β-$Co(OH)_2$, which are consistent with the values in the corresponding JCPDS standard cards $Co(OH)_2$ (JCPDS 74-1057). The diffraction peaks other than $Co(OH)_2$ were not observed, indicating the high purity of the β phase that was successfully prepared. The dried powder was calcined at different temperatures (160, 200, and 300°C), and the condition was set based on the temperature at which caloric and weight changes appeared in the Thermogravimetric Analysis (TGA)/ Differential Thermal Analysis (DTA) analysis results (Fig. 3). Fig. 2(b-d) exhibits XRD patterns of the powder obtained after heat treatment at 160, 200, and 300°C, respectively (hereafter, Co-160, Co-200, and Co-300). As shown in Fig. 2(b), it is clear that the Co_3O_4 phase coexists with CoOOH in Co-160, and the intensity of Co_3O_4 relatively increases with heat-treatment time. This aspect is also shown in Co-200 (for 1 and 3 h); on the other hand, the diffraction peak of Co-200 (for 12 h) is only associated with the Co_3O_4 phase, indicating the high purity of single crystallographic structure (Fig. 2(c)). In the case of Co-300, all diffraction peaks were matched to the Co_3O_4, and any peaks of CoOOH were not observed, as can be seen in Fig. 2(d). These results indicate that β-$Co(OH)_2$ could be oxidized in the order of CoOOH and Co_3O_4.

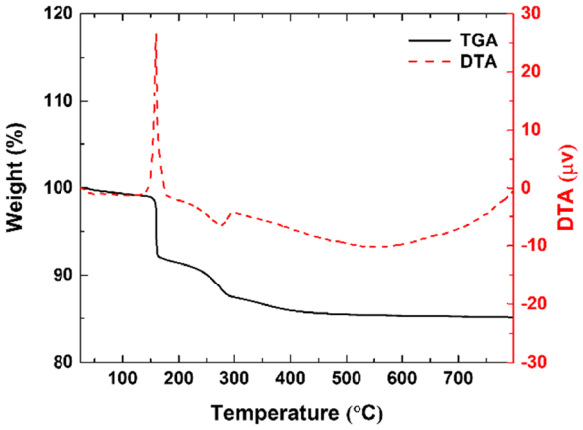

Fig. 3. TGA/DTA curves of the as-synthesized $Co(OH)_2$ powder in the temperature ranging from 25°C to 800°C in air environment

Fig. 4 shows the typical SEM images of β-$Co(OH)_2$ and Co-(160, 200, 300) powder calcined for 12 h. It seemed that the initial morphology of β-$Co(OH)_2$ are polygonal plate shapes

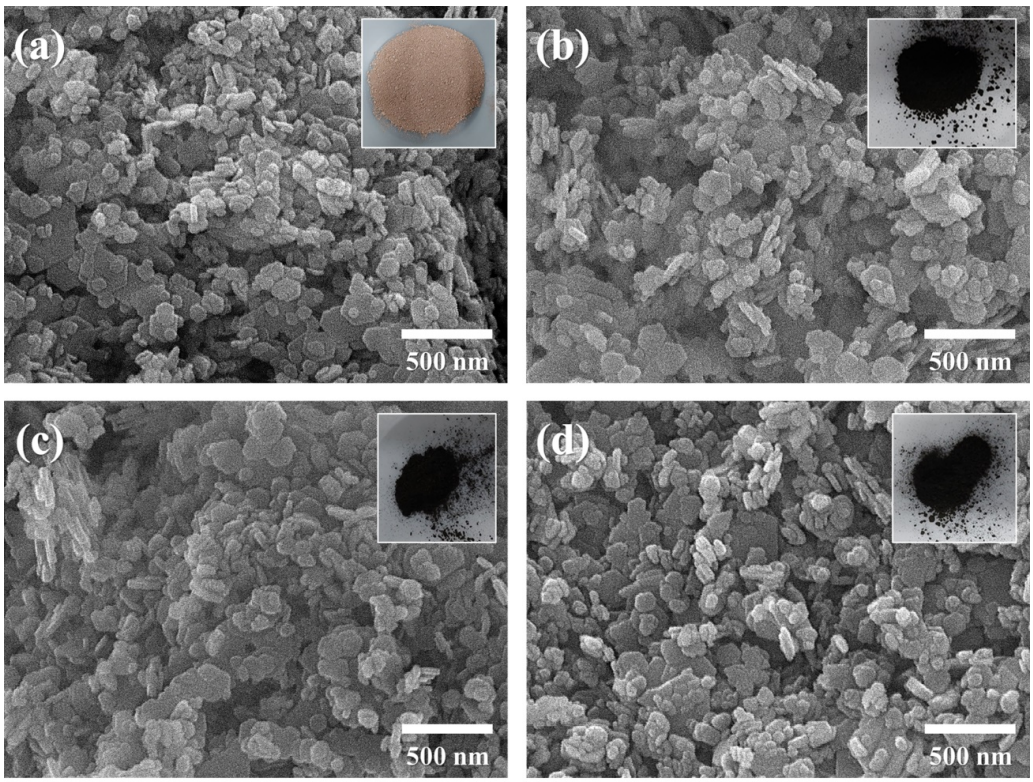

Fig. 4. SEM images of (a) pristine $Co(OH)_2$ and (b-d) the powder obtained after heat treatment at 160, 200, and 300°C for 12 h, respectively. Insets show a digital photograph of all samples

with random size (Fig. 4(a)). Furthermore, in Co-(160, 200, 300) samples, the dramatic change in both the size and shape was not found and appeared to be similar to those of β-$Co(OH)_2$, although β-$Co(OH)_2$ powder was calcined at each temperature, as can be seen in Fig. 4(b-d). It is also noted that the color of the powder changed from pink to black, indicating the oxidization of β-$Co(OH)_2$ to Co_3O_4.

To investigate the surface properties of all samples, we measured N_2 adsorption-desorption isotherms at 77 K, and the specific surface area along with BET analysis was quantitatively compared (Fig. 5(a)). As for Co-160, the surface area increased with time to 75.2, 75.1, and 95.8 m^2/g, and this trend was also revealed in Co-200 (i.e., the increase of 107.3, 107.0, and 116.1 m^2/g, respectively). On the other hand, in the case of Co-300, the surface area decreased to 100.4, 92.6, and 70.5 m^2/g. This difference between samples can be considered due to the difference in the crystal structure of $Co(OH)_2$, CoOOH, and Co_3O_4. Comparing $Co(OH)_2$ with CoOOH and Co_3O_4, the volume occupied per cobalt atom decreases. $Co(OH)_2$ (V/#Co: 0.04082 nm^3), which has a trigonal $P\bar{3}m1$ space group, recrystallizes to $R\bar{3}m$ space group when oxidized to CoOOH (V/#Co: 0.03086 nm^3). And the crystal structure changes to the cubic $Fd\bar{3}m$ symmetry when oxidation to Co_3O_4 (V/#Co: 0.02201 nm^3) [20,21]. Therefore, the shape and size of $Co(OH)_2$ are maintained during the recrystallization process, though the BET surface area can be changed because of internal nanopores generation. TABLE 1 summarizes the surface properties of all samples obtained in this work. As shown in this table, the BET surface area of Co-200 (for 12 h) was the best, and most of the pore was contributed to the nanopores with an average pore size of 3-10 nm.

Fig. 5(b) shows the typical N_2 adsorption-desorption isotherm of Co-200 (for 12 h). The profile illustrates the rapid uptake of N_2 in the p/p^0 region of 0 to 0.5, followed by a slight hysteresis; in other words, the porosity can be mainly attributed to nanopores together with little meso- and/or -macropores. This finding is further supported by the Barrett-Joyner-Halenda (BJH) pore size distribution plot, as shown in the inset of Fig. 5(b).

As mentioned, the Co_3O_4 powder with high purity and large surface area could be prepared at 200°C for 12 h (denoted as Co-200-12H); here, Co-200-12H was directly applied as the anode material for LIBs. We first measured the cyclic voltammogram (CV) to confirm the lithium electroactivity of the Co-200-12H electrode. Fig. 6(a) shows the CV curves of the Co-200-12H electrode after the first ten cycles. The first sweep commenced cathodically from the open-circuit voltage (OCV), and the peaks occurred at ~1.2 V and ~0.75 V, indicating the lithiation reaction into Co_3O_4. As a pair of redox peaks of the discharge cycle, the following charge cycle showed the anodic peaks at ~1.25 V and ~2.0 V. These CV profiles of the Co-200-12H electrode in the first ten cycles were similar to the electrochemical behavior of the previously reported Co_3O_4 [19,22,23].

Generally, it was well-known that the transition metal oxides (TMOs; M_xO_y : M = Co, Cu, Ni, Fe, etc.) have a conversion reaction mechanism with Li ($M_xO_y + ne^- + nLi^+ = xM_0 + Li_nO_y$) [24,25], thereby delivering a much higher capacity than commercial graphite (372 mAh g^{-1}) as anode material for Li-ion

TABLE 1

Summary of surface properties based on BET and BJH analysis

Sample name	Heat-treatment condition		Surface properties	
	Temp. (°C)	Time (hr)	BET surface area (m^2/g)	Pore formation
β-$Co(OH)_2$				
Co-160	160	1/3/12	75.2/75.1/95.8	Nanopore (avg. pore size of 3-10 nm)
Co-200	200	1/3/12	107.3/107.0/**116.1**	
Co-300	300	1/3/12	100.4/92.6/70.5	

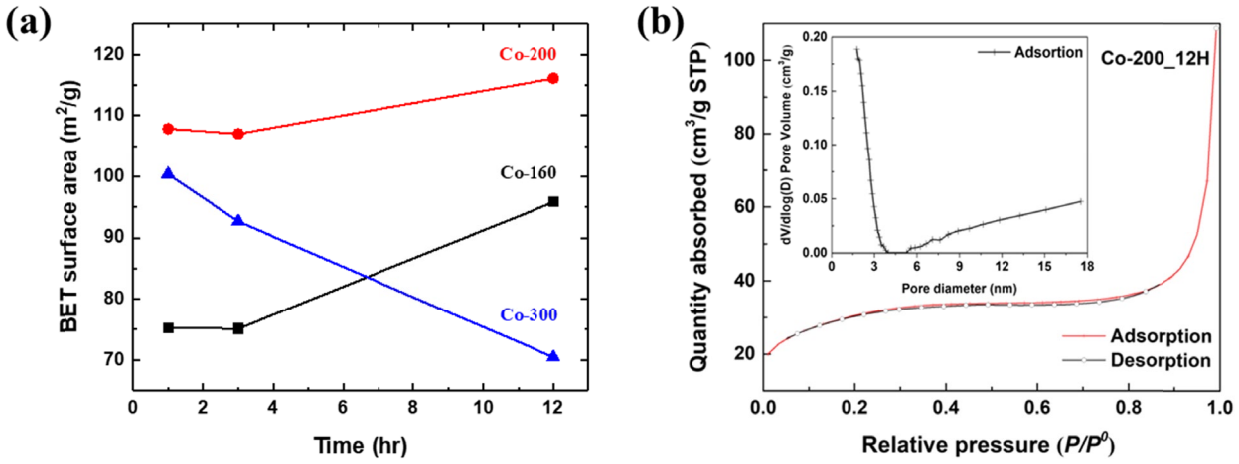

Fig. 5. (a) BET surface area plot of Co-(160, 200, 300) as a function of heat-treatment time, (b) typical N_2 adsorption-desorption isotherm profile of Co-200-12H and the pore-size distribution (the inset in (b))

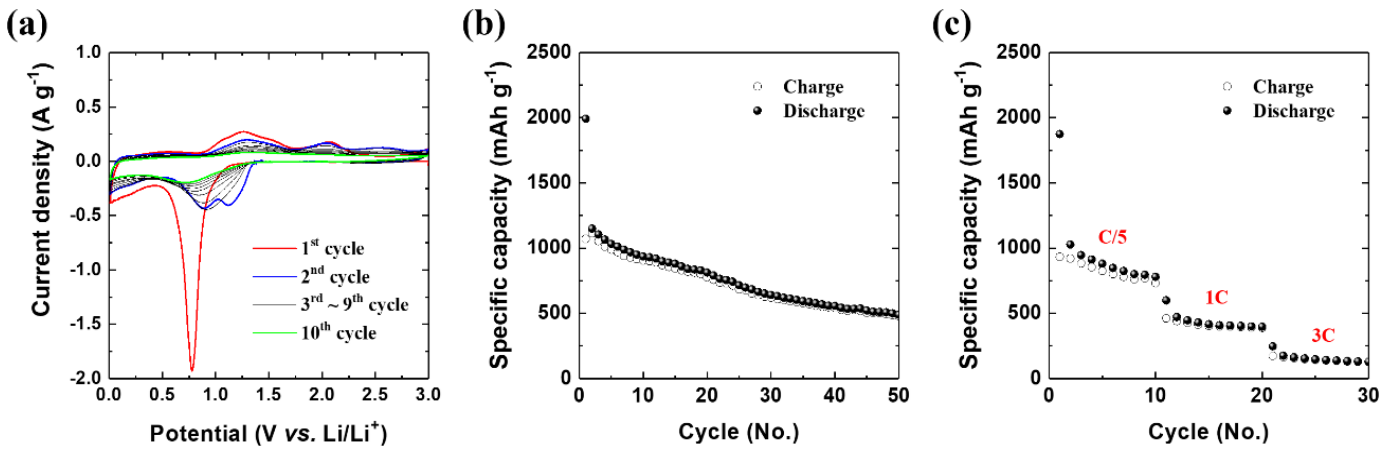

Fig. 6. Typical electrochemical properties of Co_3O_4 powder electrode. (a) CV profiles of the first ten cycles, (b) plot of specific capacity versus cycle number at a current rate of C/5, and (c) rate performance of different current rates

batteries. For this reason, TMOs have been considered promising candidates for anode materials to substitute graphite. Here, the reaction mechanism of Co_3O_4 is as follows.

$Co_3O_4 + 8Li \leftrightarrow 3Co + 4Li_2O$ (theoretical capacity of Co_3O_4 = 890 mAh g^{-1})

Fig. 6(b) shows the cyclability of the Co-200-12H electrode cycled galvanostatically at a rate of C/5 (based on the theoretical capacity of 890 mAh g^{-1} for Co_3O_4). The first discharge and charge capacities were about 3,000 mAh g^{-1} and 1,800 mAh g^{-1}, respectively, and a high reversible capacity of approximately 700 mAh g^{-1} was observed after 30 cycles. The poor capacity retention during the initial cycles may be attributed to the irreversible formation of the SEI layer. On the other hand, an excellent reversible specific capacity of over 500 mAh g^{-1} was shown after 50 cycles, indicating the high capacity and long cycle life of the Co-200-12H electrode as anode material.

In addition, the rate performance of the Co-200-12H electrode was also evaluated up to 5C. As shown in Fig. 6(c), the cell was first cycled at a current rate of C/5, and after every ten cycles, the current rate was increased in stages to 5C. The Co-200-12H electrode exhibited reversible capacities of approximately 730, 480, and 230 mAh g^{-1} at the current rates of C/5, 1C, and 3C, respectively. Even the reversible specific capacity at a current rate as high as 5C exhibited over 100 mAh g^{-1}. These electrochemical performances of the Co-200-12H electrode might be attributable to their physical good physical properties, such as a large surface area and porous properties.

4. Conclusions

Cobalt compounds were synthesized along with the recycled cobalt sulfate recovered from waste LIBs. Both cobalt hydroxide (β-$Co(OH)_2$) and cobalt oxide (i.e., CoOOH/Co_3O_4 and/or Co_3O_4) were obtained by simple precipitation and then heat treatment, respectively. The characteristics of as-prepared cobalt oxides depended on the heat-treatment temperature and time. The shape and size of $Co(OH)_2$ are maintained during the recrystallization process, but the BET surface area is changed because of internal nanopores generation. Furthermore, the Co_3O_4 powder (i.e., Co-200-12H) exhibited good electrochemical performance of both specific capacity and rate capability, which can be attributed to its enhanced surface properties, and therefore it can be possible as one of the promising candidates of anode materials for LIB.

Acknowledgments

This work was supported by the Materials & Components Technology Development Program (20011176), funded by the Ministry of Trade, Industry & Energy (MI, Korea), and by the Korea Environmental Industry & Technology Institute (KEITI) grant by the Korean government (Ministry of Environment) (No. 2022003500006, 22-9876).

REFERENCES

[1] J.Y. Mo, W. Jeon, Sustainability **10**, 2870 (2018).
[2] C.B. Tabelin, J. Dallas, S. Casanova, T. Pelech, G. Bournival, S. Saydam, Canbulat, I., Miner. Eng. **163**, 106743 (2021).
[3] E.A. Olivetti, G. Ceder, G.G. Gaustad, X. Fu, Joule **1**, 229-243 (2017).
[4] D.L. Thompson, J.M. Hartley, S.M. Lambert, M. Shiref, G.D. Harper, E. Kendrick, P. Anderson, K.S. Ryder, L. Gaines, A.P. Abbott, Green Chem. **22**, 7585 (2020).
[5] C. Peng, K. Lahtinen, E. Medina, P. Kauranen, M. Karppinen, T. Kallio, B.P. Wilson, M. Lundström, J. Power Sources **450**, 227630 (2020).
[6] H. Ali, H.A. Khan, M.G. Pecht, J. Energy Storage **40**, 102690 (2021).
[7] K. Vojisavljević, S. Wicker, I. Can, A. Benčan, N. Barsan, B. Malič, Adv. Powder. Technol. **28**, 1118 (2017).
[8] V. Bhalla, H. Tyagi, Sustain. Energy Technol. Assess. **24**, 45 (2017).
[9] L.D. Kadam, P.S. Patil, Sol. Energy Mater. Sol. Cells **70**, 15 (2001).

[10] C. Yan, Y. Zhu, Y. Li, Z. Fang, L. Peng, X. Zhou, G. Chen, G. Yu, Adv. Funct. Mater. **28**, 1705951 (2018).
[11] H. Wang, L. Zhang, X. Tan, C.M. Holt, B. Zahiri, B.C. Olsen, D. Mitlin, J. Phys. Chem. C **115**, 17599 (2011).
[12] H. Adhikari, M. Ghimire, C.K. Ranaweera, S. Bhoyate, R.K. Gupta, J. Alam, S.R. Mishra, J. Alloys Compd. **708**, 628 (2017).
[13] J. Jiang, W. Shi, S. Song, Q. Hao, W. Fan, X. Xia, X. Zhang, Q. Wang, C. Liu, D. Yan, J. Power Sources **248**, 1281 (2014).
[14] D.Y. Shin, G.H. An, H.J. Ahn, J. Powder Mater. **22** (5), 350 (2015).
[15] W. Du, R. Liu, Y. Jiang, Q. Lu, Y. Fan, F. Gao, J. Power Sources **227**, 101 (2013).
[16] K. Thangavelu, K. Parameswari, K. Kuppusamy, Y. Haldorai, Mater. Lett. **65**, 1482 (2011).
[17] M. Hassanpour, H. Safardoust-Hojaghan, M. Salavati-Niasari, J. Mol. Liq. **229**, 293 (2017).
[18] Z.Y. Li, P.T. Bui, D.H. Kwak, M.S. Akhtar, O.B. Yang, Ceram. Int. **42**, 1879 (2016).
[19] H.W. Shim, Y.H. Jin, S.D. Seo, S.H. Lee, D.W. Kim, ACS Nano **5**, 443 (2011).
[20] C.M. Hull, J.A. Koza, A. Switzer, J. Mater. Res. **31**, 3324 (2016).
[21] S. Kwon, H.T. Lee, J.H. Lee, Chem. Eur. J. **26**, 14359 (2020).
[22] K.T. Nam, D.W. Kim, P.J. Yoo, C.Y. Chiang, N. Meethong, P.T. Hammond, Y.M. Chiang, A.M. Belcher, Science **312**, 885 (2006).
[23] F. Li, Q.Q. Zou, Y.Y. Xia, J. Power Sources **177**, 546 (2008).
[24] P.L.S.G. Poizot, S. Laruelle, S. Grugeon, L. Dupont, J.M. Tarascon, Nature **407**, 496 (2000).
[25] P.L Taberna, S. Mitra, P. Poizot, P. Simon, J.M. Tarascon, Nat. Mater. **5**, 567 (2006).